

ARTICLE OPEN



Feedback-based active reset of a spin qubit in silicon

T. Kobayashi^{1,2}✉, T. Nakajima², K. Takeda², A. Noiri², J. Yoneda^{2,3} and S. Tarucha^{1,2}

Feedback control of qubits is a highly demanded technique for advanced quantum information protocols such as fault-tolerant quantum error correction. Here we demonstrate active reset of a silicon spin qubit using feedback control. The active reset is based on quantum non-demolition (QND) readout of the qubit and feedback according to the readout results, which is enabled by hardware data processing and sequencing. We incorporate a cumulative readout technique to the active reset protocol, enhancing initialization fidelity above a limitation imposed by the single-shot QND readout fidelity. An analysis of the reset protocol implies a pathway to achieve the initialization fidelity sufficient for fault-tolerant quantum computation. These results provide a practical approach to high-fidelity qubit operations in realistic devices.

npj Quantum Information (2023)9:52; <https://doi.org/10.1038/s41534-023-00719-3>

INTRODUCTION

Spin qubits based on silicon quantum dots are regarded as a powerful candidate for the building blocks of scalable quantum information processors owing to the high quantum-gate fidelities^{1–9}, high-temperature compatibility^{10,11}, and well-developed fabrication technologies^{12–14}. Fundamental technologies for a small number of qubits have matured as represented by the demonstration of a quantum error correction⁸, and technologies for scaling up toward quantum information processors have been attracting a lot of attention lately⁹. Feedback control where qubits are controlled conditionally on the results of quantum non-demolition (QND) measurements is one of the key technologies for scaling up, employed in a proposal of the surface code¹⁵. Active reset of a qubit is a basic feedback control and has been demonstrated in various qubit platforms^{16–18}. Very recently, active reset is also implemented in a silicon quantum-dot qubit system using single-shot QND measurements⁹. The fidelity of such a reset protocol can, however, be restricted by the fidelity of single-shot QND readout, which has shown limited values in past experiments in quantum-dot spin qubits except for recent reports oriented to reduction of readout errors in silicon^{19,20} and in GaAs²¹. Improvement of the reset protocol to evade limitation imposed by the QND readout infidelity will facilitate achieving the initialization fidelity over the target value >99.5% for a fault-tolerant quantum computer²².

In this work, we report feedback-based active reset of an electron spin qubit in a natural silicon quantum dot. The spin-qubit state is read out by QND measurements^{8,9,23–25}, whose outcome is used to generate a feedback pulse to reset the qubit. A combination of a digital signal processing (DSP) hardware²⁶ and a hardware sequencer (Keysight M3300A module with the option for hardware virtual instrument programming) enables us to reset the qubit much faster than spin relaxation. First, we have tested a simple reset protocol based on a single-shot QND measurement. Next, we have developed an active reset protocol based on a cumulative readout technique^{23–25}. The initialization fidelity of 98.3% has been obtained, much higher than the readout fidelity of the individual QND measurement (91.7%) which imposes a limitation for the simple reset protocol. We have also analyzed the reset protocol and propose a pathway to achieve an

initialization fidelity of >99.5%. Feedback protocols based on cumulative readout are applicable even if a high-fidelity single-shot readout is not available owing to physical and hardware constraints, providing a practical approach to qubit operations in realistic devices.

RESULTS

Active reset protocol

Figure 1a outlines an active reset protocol to initialize a qubit to the ground (spin-down) state. The protocol requires an auxiliary qubit (ancilla qubit) in addition to the qubit to be initialized (data qubit). We consider the initial two-qubit state represented as $|0_A\rangle|\psi_D\rangle$ where $|s_X\rangle$ denotes the spin-down ($s_X=0_X$) and -up ($s_X=1_X$) states of the ancilla ($X=A$) and data ($X=D$) qubits and $|\psi_D\rangle$ represents an arbitrary superposition state $\alpha|0_D\rangle + \beta|1_D\rangle$ with $|\alpha|^2 + |\beta|^2 = 1$. We first apply a QND measurement (blue area) consisting of a controlled rotation (CROT) gate using the data qubit as the control bit and a subsequent destructive readout of the ancilla qubit. The two-qubit state is first entangled to $\alpha|1_A\rangle|0_D\rangle + e^{i\phi}\beta|0_A\rangle|1_D\rangle$ by the CROT gate (ϕ is the relative phase). The subsequent destructive measurement projects the entangled state to $|0_A\rangle|1_D\rangle$ or $|1_A\rangle|0_D\rangle$ with probabilities $|\alpha|^2$ and $|\beta|^2$, and yields an ancilla measurement outcome $\mu = 0_A$ or 1_A with minimal disturbance to the data-qubit state. While this outcome just reveals the ancilla-qubit state, the two-qubit entanglement induced by the CROT gate enables us to estimate the data-qubit state at the $|0_D\rangle$ ($|1_D\rangle$) state when $\mu = 1_A$ (0_A) is obtained. Thus the ancilla outcome $\mu = 0_A$ (1_A) is interpreted as a QND estimator $m = 1_D$ (0_D) of the data-qubit state. We note that this interpretation is not unique; if the CROT gate is defined so as to entangle the qubits to $\alpha|0_A\rangle|0_D\rangle + e^{i\phi}\beta|1_A\rangle|1_D\rangle$, $\mu = 0_A$ (1_A) is interpreted as $m = 0_D$ (1_D). When $m = 1_D$ is obtained, a conditional π -rotation pulse is applied to the data qubit (yellow area). The data qubit is thus reset to the $|0_D\rangle$ state deterministically, which can be used as an input for subsequent quantum circuit.

This reset protocol relies on the QND readout and the conditioned π rotation. The initialization fidelity relates to other fidelities as $F_I = 1/2 + (2F_R - 1)F_G(2F_{QND} - 1)/2$ (See Methods). Here, F_I is the initialization fidelity, F_R is the fidelity of the QND

¹RIKEN Center for Quantum Computing, Wako, Saitama 351-0198, Japan. ²Center for Emerging Matter Science, RIKEN, Wako, Saitama 351-0198, Japan. ³Present address: Tokyo Tech Academy for Super Smart Society, Tokyo Institute of Technology, Meguro-ku, Tokyo 152-8552, Japan. ✉email: takashi.kobayashi@riken.jp

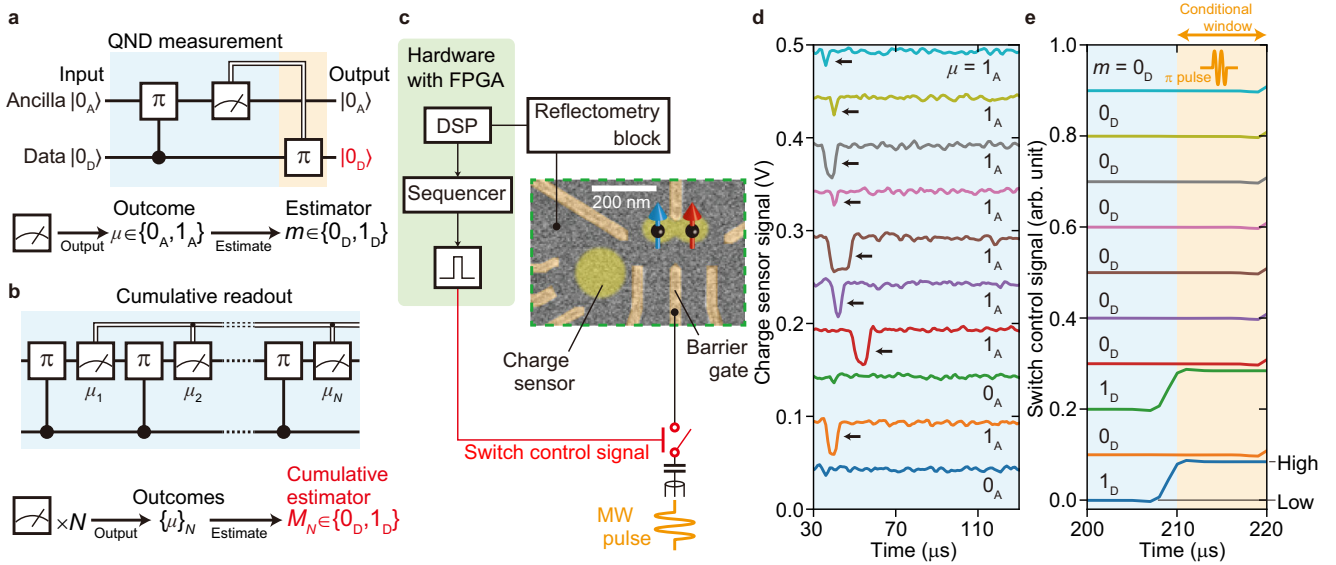


Fig. 1 Implementation of the feedback-based active reset of a spin qubit in silicon. **a** Quantum circuit showing the basic reset protocol. The QND measurement of the data qubit is implemented by the CROT gate and a destructive measurement of the ancilla qubit (blue area). The destructive measurement yields an outcome $\mu \in \{0_A, 1_A\}$ revealing the ancilla-qubit state, and the data-qubit state is estimated at the QND estimator $m \in \{0_D, 1_D\}$ according to μ (see bottom diagram). A π -rotation gate (yellow area) is applied to the data qubit when and only when the estimator $m = 1_D$. **b** Quantum circuit for cumulative readout. QND measurements are repeated N times, resulting in a set of outcomes $\{\mu\}_N = \{\mu_1, \mu_2, \dots, \mu_N\}$. A cumulative estimator $M_N \in \{0_D, 1_D\}$ for the data qubit is obtained from $\{\mu\}_N$ (see bottom diagram). **c** Schematic diagram of the experiment setup. A scanning electron micrograph image of the two-qubit device is shown in the green dashed box. **d, e** Time-domain charge sensor signals of the destructive readout (**d**), and switch control signals output after the corresponding charge sensor signals in **d** (**e**). For clarity, curves are offset from one another by 0.05 for **d** and 0.1 for **e**. Black horizontal arrows indicate dips in the charge sensor signals due to reloading of the ancilla electron from the electron reservoir. As this electron reloading event is a sign of the $|1_A\rangle$ state, we regard the presence (absence) of a dip as an ancilla measurement outcome $\mu = 1_A$ (0_A) as denoted in **d**. The obtained outcome μ is interpreted as a data-qubit estimator m . If the CROT gate entangles the ancilla and data qubit states to a form $\alpha|1_A\rangle|0_D\rangle + e^{i\phi}\beta|0_A\rangle|1_D\rangle$, $\mu = 1_A$ (0_A) is always interpreted as $m = 0_D$ (1_D) as denoted in **e**. Switch control signal is raised to the high level from 210 μs to 220 μs (yellow area) when and only when $m = 1_D$ is obtained. A π pulse applied in this time window as depicted in the top works as the conditional π pulse.

readout of the data qubit, F_{QND} is the state-preservation fidelity for the data qubit during the reset protocol (QND fidelity)²⁷, and F_G is the π -rotation fidelity. F_I , F_R , and F_{QND} are averaged over the input data-qubit states. F_R is degraded not only by errors in the destructive measurement and the preparation of the ancilla qubit but also by CROT-gate errors to map the data-qubit state on the ancilla-qubit state. In silicon spin qubits, F_R is typically much lower than F_G and F_{QND} ; in the present experiments, $F_R \leq 92\%$ and $F_{\text{QND}} \geq 99\%$ for the reset protocol based on a single-shot QND measurement as shown later. In this regime, the relation between F_I and other fidelities is approximated by $F_I \approx F_R$ and thus F_I is expected to increase with F_R in the active reset protocol.

QND readout does not perturb the measured quantity, which is its important feature allowing us to improve F_R using cumulative readout techniques^{23–25,28}. To incorporate the cumulative readout to the active reset protocol, we design a quantum circuit (Fig. 1b) to replace the single-shot QND measurement in Fig. 1a. A repetition of the measurement provides a set of ancilla measurement outcomes $\{\mu\}_N$ (N is the number of repetition). A cumulative estimator M_N of the data-qubit state is obtained from the outcome set and used to condition the subsequent π -rotation gate. We note that the cumulative estimator M_N must be calculated in real time.

Qubit system and feedback control

The ancilla and data qubits are hosted by the left and right quantum dots in a double quantum dot device^{2,24} (Fig. 1c, dashed box) with an adjacent charge sensor to detect charge occupations of the quantum dots (See Methods). An external magnetic field splits qubit levels by Zeeman energy of roughly 16 GHz (Figs. 2 and 4) or 19 GHz (Fig. 3). A micromagnet on top of the device

induces a slanting magnetic field to couple the spin qubits to the microwave (MW) voltage applied to a gate (barrier gate), which drives the ancilla and data qubits at Rabi frequencies of 2–4 MHz. The micromagnet also induces a difference in the Zeeman splittings of the ancilla and data qubits of around 600 MHz large enough to address them individually. The exchange coupling between the qubits is turned on and off by a barrier-gate pulse (see Supplementary Note 1 for details of the experimental time sequence). As the exchange coupling in the on state (6–9 MHz) is much smaller than the Zeeman splitting difference, it is effectively an Ising-type interaction²⁴ which splits the $|0_A\rangle|0_D\rangle \leftrightarrow |1_A\rangle|0_D\rangle$ and $|0_A\rangle|1_D\rangle \leftrightarrow |1_A\rangle|1_D\rangle$ transition energies. A π rotation using a MW pulse resonant to one of these transitions works as a CROT gate. The $|0_A\rangle|0_D\rangle \leftrightarrow |1_A\rangle|0_D\rangle$ ($|0_A\rangle|1_D\rangle \leftrightarrow |1_A\rangle|1_D\rangle$) transition is used for the experiments in Figs. 1, 2, 4 (Fig. 3), and thus $\mu = 0_A$ (1_A) is interpreted as $m = 1_D$ there. Here, the choice of the data-qubit projection axis in the QND measurement allows us to ignore conditional phase factors accumulated by pulsing exchange interaction. T_1 of the data qubit is >6 ms in this work. The sample is cooled down in a dilution refrigerator with a base temperature of 26 mK. The electron temperature is 36 mK measured by quantum-dot charge transition line width.

We test conditioning of the π -rotation gate to flip back the data-qubit state to $|0_D\rangle$ using a feedback scheme based on the single-shot QND measurement in the actual experimental setup (Fig. 1c). The ancilla destructive readout is performed by a combination of spin-selective tunneling²⁹ and reflectometry charge sensing. Figure 1d shows typical time-domain signals in the measurement span between 30 and 130 μs after the CROT gate. Presence of a dip (arrows) in this time span is an indication of the $|1_A\rangle$ state. The DSP hardware assigns each time trace to the ancilla measurement outcome of either $\mu = 1_A$ or 0_A using a single threshold value (see

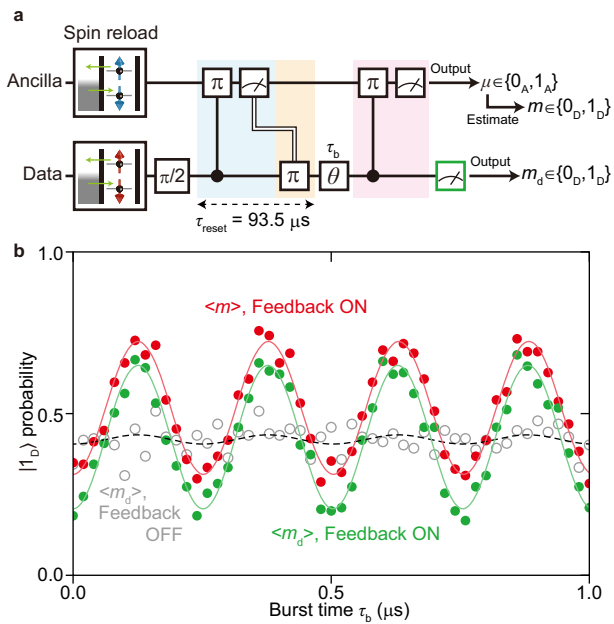


Fig. 2 Test of the active reset. **a** Quantum circuit to test the reset protocol. The data and ancilla qubits are initialized at the beginning by reloading electrons from reservoirs. The data qubit is also subjected to a $\pi/2$ rotation before the active reset protocol. After the active reset, a θ rotation by a resonant MW burst for τ_b is applied to the data qubit. Finally, the data-qubit state is read out by a QND measurement (red area) and a subsequent destructive measurement to the data qubit (green square). The data-qubit state is estimated at an estimator $m = 0_D$ (1_D) when the ancilla outcome $\mu = 1_A$ (0_A) is obtained by the ancilla destructive measurement. Separately, the data qubit is directly read out by the final destructive measurement, whose outcome is denoted m_d . **b** Rabi oscillations measured with and without the feedback as a function of τ_b . The red circles show the QND estimator $\langle m \rangle$ ($\langle \dots \rangle$ denotes ensemble averaging). The green and open circles show $\langle m_d \rangle$. The solid and dashed curves are the fit curves for the data measured with and without the feedback, respectively.

Fig. 1d), and then to a data-qubit estimator m of 1_D for $\mu = 0_A$ and 0_D for $\mu = 1_A$, respectively (Fig. 1e). The state of a MW switch placed on the output port of a MW generator is decided by the value of m , enabling the conditional π -rotation gate on the data qubit in 210 μ s. The time delay includes readout time (100 μ s), sequencing time (80 μ s), wait time to stabilize the charge sensor signal (20 μ s), and wait times (10 μ s in total). We note that these times are shortened in the following experiments (see Supplementary Note 1 for details of the experimental time sequence). Figure 1e shows the switch control signal following each of the readout signals shown in the same color as in Fig. 1d.

Implementation of the active reset using single-shot QND readout

We now demonstrate the qubit reset protocol using the QND measurement and the feedback scheme. Figure 2a shows the quantum circuit used. Before the reset protocol, the ancilla and data qubits are prepared in the $|0_D\rangle$ and $|0_A\rangle$ states by reloading an electron with down spin to each quantum dot. The data qubit is subsequently subjected to a $\pi/2$ pulse, which makes a superposition state of the $|0_D\rangle$ and $|1_D\rangle$ states. The following QND measurement at the beginning of the reset protocol randomly projects the data-qubit state to $|0_D\rangle$ or $|1_D\rangle$, which works as an unbiased input state. The data qubit is then reset to the $|0_D\rangle$ state using the active reset protocol described in the last section. To analyze the fidelity of the reset protocol, we apply a

Rabi rotation with an angle θ to the data qubit by a resonant MW burst for duration τ_b . After the Rabi rotation, the data qubit is read out by two independent measurements, a QND measurement followed by a destructive one (see Fig. 2a). The QND measurement, which is performed in the same manner as that used to generate feedback, yields a QND estimator m of the data qubit. The destructive measurement of the data qubit, on the other hand, yields an outcome m_d directly revealing the data-qubit state. Analyzing the joint probabilities of m and m_d allows one to obtain the initialization and readout fidelities^{23,24}. Here time taken by the reset protocol τ_{reset} is 93.5 μ s measured from the CROT gate to the conditional π rotation.

Figure 2b shows Rabi oscillations of the data qubit exhibited by the data-qubit destructive-measurement outcome $\langle m_d \rangle$ (green) and the QND estimator $\langle m \rangle$ (red). Here, $\langle \dots \rangle$ denotes ensemble averaging. For comparison, we also perform measurements without the conditional π -rotation pulse for the active reset (open circles). The data set with feedback shows clear Rabi oscillations with visibility of $44 \pm 3\%$ and $41 \pm 2\%$ for m_d and m , respectively (from fitting, solid curves). The oscillation offsets of $\langle m_d \rangle$ and $\langle m \rangle$ reflect the destructive measurement error rates of the ancilla and data qubits, respectively, and are thus slightly different. We note that the Rabi oscillation with a low visibility ($3 \pm 2\%$, dashed curve) is observed in m_d without the feedback because of a small remnant of bias in the initial data-qubit state. This result indicates successful initialization of the data qubit by the reset protocol.

The Rabi-oscillation visibility in $\langle m \rangle$ ($\langle m_d \rangle$) depends not only on the initialization fidelity F_I but also on the QND (destructive) readout fidelities $f_{R,s}$ ($f_{d,R,s}$), where the subscript s denotes the prepared data-qubit state ($|0_D\rangle$ for $s=0$ and $|1_D\rangle$ for $s=1$). To separately estimate these fidelities, we analyze the joint probabilities $P(m, m_d)$ of obtaining a combination of m and m_d rather than the mean values $\langle m_d \rangle$ and $\langle m \rangle$ ^{23,24} (see Methods and Supplementary Note 2 for the joint probability analyses). We obtain $F_I = 81.1 \pm 0.6\%$ along with the readout fidelities $f_{R,0} = 85.1 \pm 0.9\%$, $f_{R,1} = 83 \pm 1\%$, $f_{d,R,0} = 95 \pm 1\%$, and $f_{d,R,1} = 70.6 \pm 0.9\%$. The average fidelity F_R of the QND readout for feedback is $(f_{R,0} + f_{R,1})/2 = 84 \pm 1\%$. The F_I value close to F_R implies that F_I is limited by F_R .

The destructive measurement of the data qubit used in Fig. 2a requires an electron reservoir²⁹, which imposes geometrical constraints for scaling up. One of the benefits of the active reset protocol is that a qubit can be initialized without reloading an electron from reservoirs. To demonstrate this, we implement a quantum circuit shown in Fig. 3a without the destructive measurement of the data qubit. τ_{reset} is 93 μ s out of 100 μ s taken by each cycle. Figure 3b shows Rabi oscillations exhibited by m similarly to Fig. 2b. Clear difference between presence (blue) and absence (gray) of the reset pulse corroborates the success of the active reset protocol. The data qubit is free from electron reload throughout the experiment in contrast to Fig. 2a, while a note should be taken that the ancilla qubit still uses electron reload for a destructive measurement. The electron reload can be avoided completely by using Pauli spin blockade readout as demonstrated in ref. 9, although an additional ancilla spin is required for a QND measurement.

Feedback using cumulative readout

F_I obtained by the active reset protocol in Fig. 2a is limited by the low f_R value of the QND measurement. We attempt to incorporate a cumulative readout technique to improve the readout fidelity^{23–25} in the active reset protocol. Increase of the readout fidelity by cumulative readout is tested using a quantum circuit shown in Fig. 3c. After the reset protocol and the spin rotation, the data qubit is read out 21 times (instead of once as in Fig. 3a) in a QND manner. Here we use only the last QND measurement outcome for active reset, but we use the rest of the ancilla readout outcomes, $\{\mu\}_{20}$, to analyze the cumulative readout process.

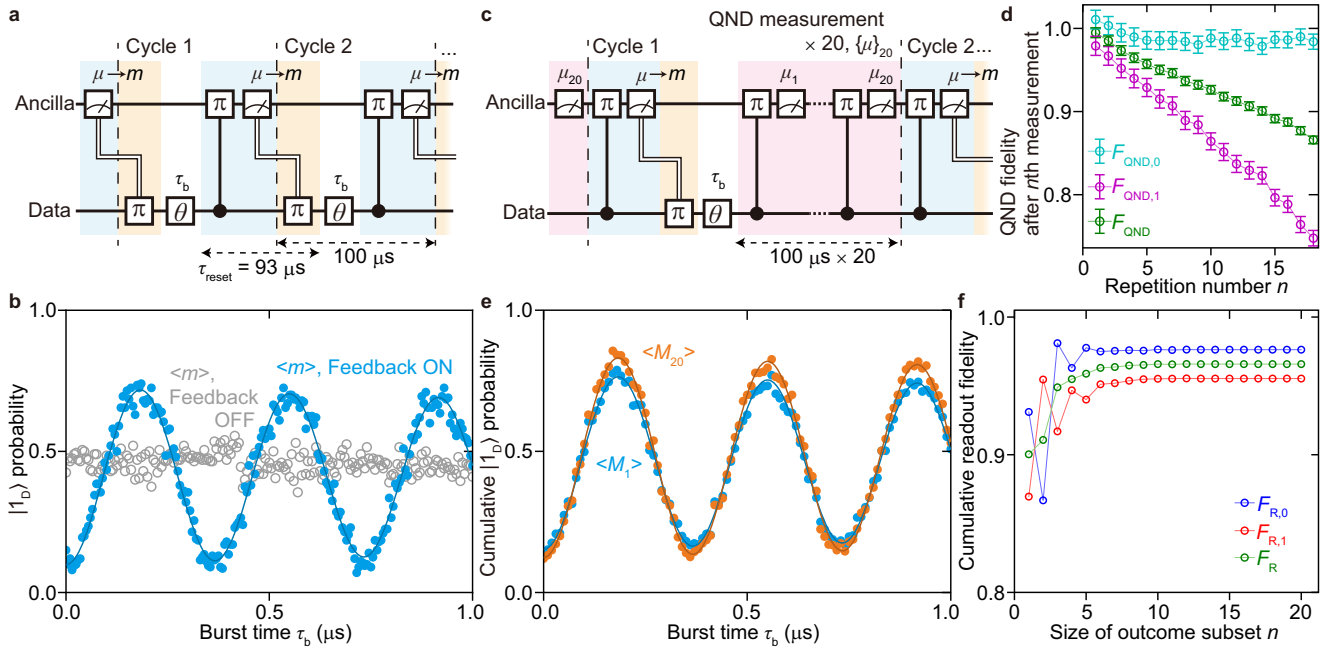


Fig. 3 Active reset without electron reload to the data qubit and improvement of the readout fidelities by the repetitive QND measurements. **a** Quantum circuit to test the reset protocol without access of the data-qubit to the electron reservoirs. The circuit repeats a cycle consisting of a QND measurement, a conditional π pulse, and a θ rotation pulse to the data qubit. The ancilla qubit is initialized after each destructive measurement using access to the reservoir. **b** Rabi oscillations measured with and without the feedback (solid and open circles, respectively). **c** Quantum circuit with a cumulative readout sequence (red area) to measure the final data-qubit state. In addition to the circuit in **a**, a 20-fold repetition of QND measurement is inserted before the single QND measurement to generate feedback. **d** QND fidelities after the n th QND measurement for the $|0_D\rangle$ and $|1_D\rangle$ states, $F_{\text{QND},0}$ and $F_{\text{QND},1}$, and their average F_{QND} , estimated by analyzing the joint probability. The solid lines are eye guides. The error bars represent 1σ confidence intervals obtained from fitting. **e** Rabi oscillations measured by the cumulative readout. Each plot is obtained by the Bayesian estimation using subsets $\{\mu\}_n$ ($n=1$ and 20) of the set of repetitive measurement outcomes $\{\mu\}_{20}$ (blue and orange, respectively). The solid curves are sinusoidal fit results. **f** Cumulative readout fidelities for the $|0_D\rangle$ and $|1_D\rangle$ states, $F_{R,0}$ and $F_{R,1}$, and their average F_R as a function of the subset size n . The solid lines are eye guides.

A major drawback of cumulative readout is the time taken by the repetitive QND measurements, where spin relaxations can induce errors in preservation of the data-qubit state during the readout. Here we compare gains in the readout fidelity and losses of the QND fidelity in the cumulative readout process. First, fidelities of each QND measurement are extracted by analyzing joint probabilities $P(m_k, m_{20})$ where m_k ($k=1, 2, \dots, 20$) is the estimator for the data-qubit state obtained from the single outcome μ_k . We obtain fidelities of the individual QND measurement for the $|0_D\rangle$ and $|1_D\rangle$ states, $f_{R,0} = 93.6 \pm 0.1\%$, $f_{R,1} = 89.1 \pm 0.2\%$ (averaged over k), and their average $f_R = 91.4 \pm 0.1\%$ (see Supplementary Note 2 for the joint probability analyses). From the k dependence of $P(m_k, m_{20})$, we can extract the initialization fidelity $F_1 = 87.8 \pm 0.2\%$ and the lifetimes of the $|0_D\rangle$ and $|1_D\rangle$ states, $T_{1,0} = 80 \pm 20$ ms and $T_{1,1} = 6.6 \pm 0.1$ ms. We can also extract the QND fidelities after n -fold repetition of the QND measurement for the $|0_D\rangle$ and $|1_D\rangle$ states, $F_{\text{QND},0}$ and $F_{\text{QND},1}$, and their average F_{QND} (Fig. 3d). Using a Bayesian estimation method taking these T_1 values into account, we calculate cumulative estimators M_n for the data-qubit state before the measurement from subsets $\{\mu\}_n = \{\mu_1, \mu_2, \dots, \mu_n\}$ ($n \leq 20$) of the $\{\mu\}_{20}$ (see Supplementary Note 3 for the analyses of the repetitive measurement outcomes). Figure 3e shows the Rabi oscillations obtained from the estimators M_n for $n=1$ and 20 (blue and orange). The Rabi-oscillation visibility for $n=20$ is $>n=1$, implying improved readout fidelities by cumulative readout. Given $F_1 = 87.8\%$, we can estimate the cumulative readout fidelities for the $|0_D\rangle$ and $|1_D\rangle$ states, $F_{R,0}$ and $F_{R,1}$, and their average F_R as a function of n (Fig. 3f). F_R increases with n for $n < 10$ and saturates to $97.1 \pm 0.6\%$ for higher n , and is indeed improved by the cumulative readout technique in comparison with single-shot

QND readout. However, the F_{QND} values are much lower than F_R for $n > 10$ ($F_{\text{QND}} = 92.6 \pm 0.5\%$ at $n = 11$). In this case, the fidelity of active reset may be limited by F_{QND} and hardly be improved by the incorporation of cumulative readout to the active reset protocol. To effectively incorporate cumulative readout to active reset, we improve F_{QND} by changing the experimental condition to prolong the data-qubit lifetimes.

Figure 4a shows an implementation of the active reset based on the cumulative readout. We change gate biases and find a condition with the longer spin relaxation times. The single-shot QND readout to generate feedback in Fig. 3c is replaced by an 11-fold repetition of the QND measurement. To cumulatively estimate the data-qubit state in real time on the hardware sequencer, we implement an online Bayesian-estimation block where the cumulative estimator is computed in the course of the repetitive measurement. Each ancilla outcome is used for the computation immediately after its acquisition, which reduces computational time after the measurement repetition and is also suitable for the hardware sequencer with a limited number of registers. These features are in contrast to the Bayesian estimation used in Fig. 3e, which is executed after all data have been recorded to standard computer storage. After the 11th QND measurement, the cumulative estimator M_{11} is provided by the Bayesian-estimation block and used to generate feedback to condition the π rotation for active reset. The Bayesian-estimation block takes likelihood parameters into account but not T_1 values for the sake of simplicity. While the individual cycle of the repetition is reduced to $65 \mu\text{s}$ from $100 \mu\text{s}$ in Fig. 3c, τ_{reset} is increased to $708 \mu\text{s}$ due to the repetitive measurements. We also perform another 20-fold repetition of the QND measurements and acquire $\{\mu\}_{20}$ for analysis.

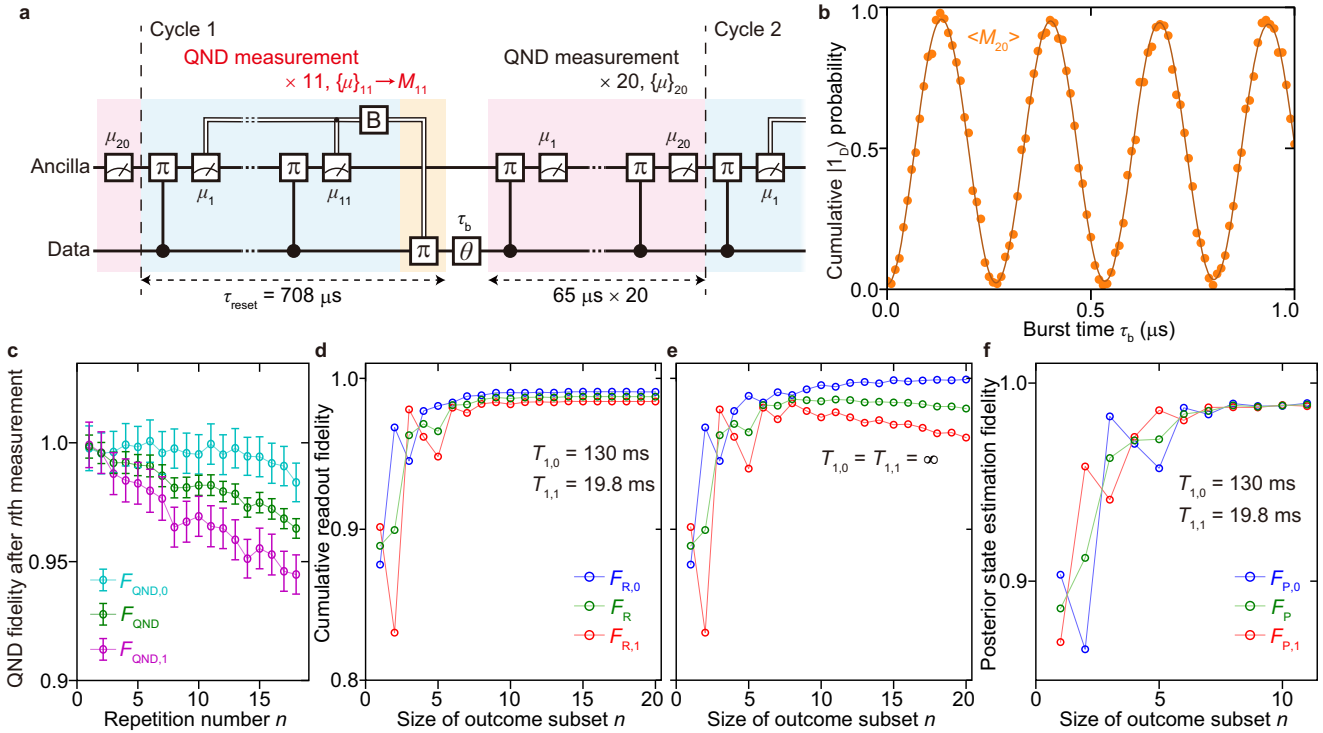


Fig. 4 Feedback using a Bayesian-estimation logic. **a** Quantum circuit to test the reset protocol using a cumulative QND readout. The difference from the circuit shown in Fig. 3c is that the single QND measurement to generate feedback is replaced by a 11-fold repetition of QND measurement (blue area). Outcomes $\{\mu\}_{11}$ of the repetitive measurements are fed to the online Bayesian-estimation block (Box denoted B) and feedback is generated according to the resulting cumulative estimator M_{11} . After the data qubit is reset and rotated resonantly, another cumulative readout sequence with 20 QND measurements (red area) is carried out to measure the data-qubit state. **b** Rabi oscillations estimated by the Bayesian method using the set of ancilla measurement outcomes $\{\mu\}_{20}$. The Bayesian estimation takes $(T_{1,0}, T_{1,1}) = (130 \text{ ms}, 19.8 \text{ ms})$ into account. **c** QND fidelities after the n th QND measurement for the $|0_D\rangle$ and $|1_D\rangle$ states, $F_{\text{QND},0}$ and $F_{\text{QND},1}$, and their average F_{QND} , estimated by analyzing the joint probability. The solid lines are eye guides. The error bars represent 1σ confidence intervals obtained from fitting. **d, e** Cumulative readout fidelities for the $|0_D\rangle$ and $|1_D\rangle$ states, $F_{R,0}$ and $F_{R,1}$, and their average F_R estimated with using $(T_{1,0}, T_{1,1}) = (130 \text{ ms}, 19.8 \text{ ms})$ (**d**) and $(T_{1,0}, T_{1,1}) = (\infty, \infty)$ (**e**). **f** Estimation fidelities for the data-qubit state after the n th QND measurement for the $|0_D\rangle$ and $|1_D\rangle$ states, $F_{P,0}$ and $F_{P,1}$, and their average F_P .

Joint probability analysis of $\{\mu\}_{20}$ in the same manner as Fig. 3c-f reveals improved $T_{1,0} = 130 \pm 30 \text{ ms}$ and $T_{1,1} = 19.8 \pm 0.7 \text{ ms}$ together with the single-shot QND readout fidelity f_R of $91.7 \pm 0.2\%$ ($f_{R,0} = 89.9 \pm 0.2\%$ and $f_{R,1} = 93.5 \pm 0.2\%$) comparable with that in Fig. 3. Along with these parameters, we obtain the F_I value of $98.33 \pm 0.08\%$ much $>87.8\%$ in Fig. 3c-e. This initialization fidelity is also higher than the single-shot QND readout fidelity f_R limiting F_I in the simple reset protocol (Figs. 2a and 3a, c), indicating the superior accuracy of the active reset protocol in Fig. 4a. We also note that this F_I value is comparable to a recent report of qubit preparation using real-time monitoring of negative-result measurements in silicon ($98.9 \pm 0.4\%$)³⁰. As a result of the improved initialization fidelity, we can observe Rabi oscillations with a higher visibility in Fig. 4b than in Fig. 3e. Incorporating cumulative readout to generate feedback certainly helps to improve the fidelity of the active reset protocol.

We review the effect of spin relaxation during the repetitive measurement, which is ignored in the online Bayesian estimation. Figure 4c shows the QND fidelities $F_{\text{QND},0}$, $F_{\text{QND},1}$, and F_{QND} extracted by the joint probability analysis. The observed F_{QND} ($98.2 \pm 0.4\%$ at $n = 11$) is likely to limit F_I , while higher than Fig. 3d and the previous report²⁴. We also calculate the readout fidelities $F_{R,0}$, $F_{R,1}$, and F_R from the data set $\{\mu\}_{20}$. Using $T_{1,0} = 130 \text{ ms}$ and $T_{1,1} = 19.8 \text{ ms}$ for a Bayesian estimation, the cumulative readout for the data-qubit state just after the θ rotation yields $F_R = 98.7 \pm 0.5\%$ at $n = 11$ (Fig. 4d), which is slightly $>F_{\text{QND}}$. Notably, the saturation of fidelities at large n is attributed to QND errors, and thus the higher QND fidelities should improve F_R . Since

the Bayesian method used to generate feedback does not take the QND errors into account, we also inspect the cumulative readout fidelities estimated by a Bayesian method assuming infinitely long T_1 values (Fig. 4e). While the $F_{R,0}$ and $F_{R,1}$ values deviate from each other, this estimation method provides a close F_R value to Fig. 4d ($F_R = 98.6 \pm 0.8\%$ at $n = 11$). Based on these considerations, the initialization fidelity is now mainly limited by the spin relaxation effect and likely to further increase with the QND fidelities.

Online Bayesian estimation taking T_1 values into account, which is not implemented in this work, enables to estimate the data-qubit state after the repetitive measurement (posterior state)²⁴. Here, estimating the posterior state using the outcome set $\{\mu\}_{20}$, we assess performance of the active reset protocol based on the online posterior-state estimation. Figure 4f shows the fidelities of the posterior-state estimation for the $|0_D\rangle$ and $|1_D\rangle$ states and their average, $F_{P,0}$, $F_{P,1}$, and F_P from the data set $\{\mu\}_{20}$ in a similar way to ref. ²⁴. The evaluated F_P value ($98.9 \pm 0.8\%$ at $n = 11$) is, however, comparable with the observed F_I value, indicating that active reset based on the posterior-state estimation does not improve F_I . The saturation of F_P at $n \geq 7$ implies that the posterior-state estimation fidelity is poisoned by the QND errors (similarly to F_R for the large n values). The high QND fidelities are an essential requirement even for active reset based on the posterior-state estimation.

DISCUSSION

Reduction of the time consumed by the reset protocol is important since a shorter reset time enables various applications.

In this work, we can decrease τ_{reset} for the reset protocol using the single-shot QND measurement (Fig. 3a) to $\approx 60 \mu\text{s}$, which is mainly limited by the destructive readout taking $40 \mu\text{s}$. The energy-selective readout is generally limited in terms of the readout speed as it relies on stochastic electron exchange between a quantum dot and an electron reservoir. By employing the spin readout based on Pauli spin blockade, the readout time can be decreased to $1 \mu\text{s}$ with high fidelity^{19,31–33}. The second dominant limitation is the time taken by operation of the hardware sequencer. As this takes slightly $>10 \mu\text{s}$ in the present setup, we reserve $15 \mu\text{s}$ before the application of the reset pulse (see Supplementary Note 1 for details of the experimental time sequence). We suppose this latency is due to the sequencing hardware and expect that it can be reduced to $<1 \mu\text{s}$ as demonstrated in ref. 9. These potential improvements will decrease τ_{reset} for feedback based on a single-shot QND measurement to $2 \mu\text{s}$ or less.

Incorporation of the cumulative readout to the feedback-based reset is a reasonable way to enhance F_I exceeding the target value of 99.5% for fault-tolerant quantum computation²² for a given single-shot QND readout fidelity. While the time-consuming repetition of the QND measurement is a drawback of this scheme, a numerical simulation predicts that three-fold repetition provides $F_R > 99.9\%$ if the readout fidelity of the individual QND measurement is 99%²³. Together with the short readout time ($1 \mu\text{s}$) and the short sequencing time ($<1 \mu\text{s}$), this enables to perform high fidelity cumulative readout with τ_{reset} of $6 \mu\text{s}$. Such a short τ_{reset} would yield $F_{\text{QND}} > 99.98\%$ using the T_1 values observed in Fig. 4. The fidelity of the active reset protocol is then expected to be $F_I > 99.5\%$ for $F_G > 99.2\%$. As the single-qubit gate fidelity of 99.5% is routinely obtained in state-of-the-art spin qubits in silicon^{1–9}, the fidelity of the π -rotation gate rarely prevents F_I from reaching the target value. Therefore, we anticipate that $F_I > 99.5\%$ is achievable by improving each QND readout fidelity and shortening the reset protocol.

In conclusion, we have demonstrated a deterministic initialization scheme of a spin qubit based on the QND measurement. Combination of fast data processing and sequencing enables us to implement feedback according to the QND-readout estimators before the data-qubit state relaxes. This scheme works properly regardless of isolation of a qubit from the electron reservoirs. We also demonstrate that cumulative readout techniques can be incorporated to improve the initialization fidelity by the reset protocol. This scheme opens a pathway to develop silicon spin quantum information architectures suitable for scaling up demanded for quantum information processors.

METHODS

Initialization fidelity of the active reset protocol

The averaged initialization fidelity F_I of the active reset protocol to the $|0_D\rangle$ state is expressed as follows:

$$F_I = \frac{F_{I,0} + F_{I,1}}{2}, \quad (1)$$

$$1 - F_{I,0} = F_{R,0}(1 - F_{\text{QND},0}) + (1 - F_{R,0})F_G F_{\text{QND},0} + (1 - F_{R,0})(1 - F_G)(1 - F_{\text{QND},0}), \quad (2)$$

$$1 - F_{I,1} = (1 - F_{R,1})F_{\text{QND},1} + F_{R,1}F_G(1 - F_{\text{QND},1}) + F_{R,1}(1 - F_G)F_{\text{QND},1}. \quad (3)$$

Here, $F_{I,s}$, $F_{R,s}$ and $F_{\text{QND},s}$ are the initialization, readout and QND fidelities for a given data-qubit state $|s_D\rangle$ ($s = 0, 1$), respectively, and F_G is the fidelity of the conditional π rotation applied to the data qubit. Substituting the second and third equations to the first

one, we obtain

$$F_I = \frac{1 + F_{\text{QND},0} - F_{\text{QND},1} - F_G(2F_{\text{QND},0} - 1)}{2} + \frac{1}{2}F_{R,0}F_G(2F_{\text{QND},0} - 1) + \frac{1}{2}F_{R,1}F_G(2F_{\text{QND},1} - 1). \quad (4)$$

Using $F_R = (F_{R,0} + F_{R,1})/2$ and $F_{\text{QND}} = (F_{\text{QND},0} + F_{\text{QND},1})/2$,

$$F_I = \frac{1}{2} + \frac{1}{2}(2F_R - 1)F_G(2F_{\text{QND}} - 1) + \frac{1}{2}\{(F_{R,0} - F_{R,1})F_G + (1 - F_G)\}(F_{\text{QND},0} - F_{\text{QND},1}). \quad (5)$$

According to the values of F_R and F_{QND} presented in the main text, the second term is comparable with $1/2$ for $F_G \approx 1$. We also find that $F_{R,0} - F_{R,1} < 1$ (4.5% for the single-shot QND measurement in Figs. 3 and 1% for the cumulative readout based on 11 QND measurements in Fig. 4) and $F_{\text{QND},0} - F_{\text{QND},1} < 1$ (1.4% in Figs. 3 and 2.8% in Fig. 4) in our experiments. Also assuming $F_G \approx 1$, the third term is $< 10^{-3}$. Thus we neglect the third term and obtain

$$F_I = \frac{1}{2} + \frac{1}{2}(2F_R - 1)F_G(2F_{\text{QND}} - 1). \quad (6)$$

In the above argument, we assume that the data-qubit state at the input to the reset protocol is prepared to the $|0_D\rangle$ state or the $|1_D\rangle$ state randomly with equal probability. This is not the case in the experiments presented in Figs. 3 and 4, since the input data-qubit state may be strongly correlated to the final data-qubit state of the previous cycle. For the case of general input data-qubit states, the initialization fidelity is represented by using the probability of the $|1_D\rangle$ state before the reset protocol (denoted by the dashed vertical lines in Figs. 3a, c and 4a), $p_{0,1}$:

$$F'_I = (1 - p_{0,1})F_{I,0} + p_{0,1}F_{I,1} = F_{I,0} + p_{0,1}\delta F_I, \quad (7)$$

using $\delta F_I = F_{I,1} - F_{I,0}$. If the initialization fidelity is state dependent ($\delta F_I \neq 0$), the second term must be considered in estimation of F_I . However, below we argue that the state dependence is negligible ($\delta F_I = 0$) in the present experiment. Since the data qubit is not subject to spin reload between each Rabi burst and reset protocol, $p_{0,1}$ is approximated as $p_{0,1} \approx F_{\text{QND},1}p_1(\tau_b) + (1 - F_{\text{QND},0})(1 - p_1(\tau_b))$. Here, $F_{\text{QND},0}$ and $F_{\text{QND},1}$ are the values for 20-fold repetitive measurements to account for the QND fidelities in the red area in Figs. 3c and 4a while unity for Fig. 3a. $p_1(\tau_b)$ is the asymptotic value of the probability of the $|1_D\rangle$ state just after the θ rotation, satisfying

$$p_1(\tau_b) = F'_I \gamma_{\text{Rabi}}(\tau_b) + (1 - F'_I)(1 - \gamma_{\text{Rabi}}(\tau_b)) = \frac{1}{2} + \frac{1}{2}(2F_{I,0} + 2p_{0,1}\delta F_I - 1)(2\gamma_{\text{Rabi}}(\tau_b) - 1), \quad (8)$$

where $\gamma_{\text{Rabi}}(\tau_b) = 1/2 - \cos(2\pi f_{\text{Rabi}}\tau_b)\exp(-\tau_b/T_{2,\text{Rabi}})/2$ is the transition probability from the $|0_D\rangle$ state to the $|1_D\rangle$ state for the θ rotation. Solving this equation for $p_1(\tau_b)$, we obtain

$$p_1(\tau_b) = \frac{1}{2} + \frac{1}{2} \frac{2F_I - 1 + \delta F_I \delta F_{\text{QND}}}{2F_I - 1 - (2\gamma_{\text{Rabi}}(\tau_b) - 1)(2F_{\text{QND}} - 1)\delta F_I} (2\gamma_{\text{Rabi}}(\tau_b) - 1). \quad (9)$$

Here $\delta F_{\text{QND}} = F_{\text{QND},1} - F_{\text{QND},0}$. The oscillating component $\gamma_{\text{Rabi}}(\tau_b)$ in the denominator induces higher harmonics of f_{Rabi} , which is apparent in the Taylor expansion of $p_1(\tau_b)$ for δF_I

$$p_1(\tau_b) = \frac{1}{2} + \frac{1}{2}(2F_I - 1 + \delta F_{\text{QND}}\delta F_I)(2\gamma_{\text{Rabi}}(\tau_b) - 1) + \frac{1}{2}(2F_{\text{QND}} - 1)(2F_I - 1)(2\gamma_{\text{Rabi}}(\tau_b) - 1)^2\delta F_I + O(\delta F_I^2). \quad (10)$$

The $|1_D\rangle$ probability shown in Figs. 3b, d, and 4b is described by this equation. However we do not observe $2f_{\text{Rabi}}$ oscillations attributed to the third term, indicating that δF_I is small in the experiments. We therefore neglect the state dependence of the initialization fidelity in the analysis of Figs. 3 and 4.

Experimental parameters

The device is a double quantum dot fabricated on a silicon/silicon-germanium heterostructure with the natural isotope abundance, which was investigated in previous reports^{2,24}. Charge occupations of the double dot are read by a radio-frequency reflectometry technique with the charge sensor neighboring the left quantum dot^{31,32}. The carrier frequency is 205 MHz and the carrier power at the output port of a radio-frequency signal generator is 13 dBm, which is attenuated to ≈ -100 dBm before the device by an attenuator chain. The external magnetic field is 0.49 T (Figs. 2 and 4) or 0.60 T (Fig. 3). Zeeman splitting is 15.448 GHz (Fig. 2), 18.581 GHz (Fig. 3), and 15.438 GHz (Fig. 4) for the ancilla qubit when the exchange interaction is turned on, and is 16.006 GHz (Fig. 2), 19.156 GHz (Fig. 3), and 16.033 GHz (Fig. 4) for the data qubit when the exchange interaction is turned off. The difference in the Zeeman splittings of the ancilla and data qubits is around 600 MHz. The exchange coupling in the on state is 9.0 MHz (Fig. 2), 8.9 MHz (Fig. 3), and 6.1 MHz (Fig. 4). The Rabi frequency of the ancilla qubit is 2.8 MHz (Figs. 2), 2.2 MHz (Fig. 3), and 2.0 MHz (Fig. 4). The $|0_A\rangle|0_D\rangle \leftrightarrow |1_A\rangle|0_D\rangle$ and $|0_A\rangle|1_D\rangle \leftrightarrow |1_A\rangle|1_D\rangle$ transitions are used for the CROT gate in Figs. 2, 4 and Fig. 3, respectively. The sizes of the exchange interaction and the ancilla Rabi frequency are not exactly tuned to cancel out the ancilla off-resonance drive in the CROT gate, which slightly decreases F_R of an individual QND measurement. In the experiments, the device is operated near the charge-symmetry point of the double dot to decouple the qubits from noise in energy level detuning. Dephasing time T_2^* is ~ 1 μ s for both qubits.

Fundamentals of the joint probability analysis

Assuming that the destructive and the QND measurement in Fig. 2a is stochastically independent of each other, the joint probability $P(m, m_d)$ is expressed in a form where the infidelities in initialization and readout of the qubit state are separated^{23,24}:

$$P(m, m_d) = \{1 - p(\tau_b)\} \Theta_{0,m}(f_{R,0}) \Theta_{0,m_d}(f_{d,R,0}) + p(\tau_b) \Theta_{1,m}(f_{R,1}) \Theta_{1,m_d}(f_{d,R,1}). \quad (11)$$

Here, $\Theta_{0,m}(x) = x$ for $m = 0_D$ and $\Theta_{0,m}(x) = 1 - x$ for $m = 1_D$, and always $\Theta_{1,m}(x) = 1 - \Theta_{0,m}(x)$. $p(\tau_b)$ is the $|1_D\rangle$ -state probability after the θ rotation induced by a resonant MW burst for duration τ_b , modeled as $p(\tau_b) = B - \text{Acos}(2\pi f_{\text{Rabi}}\tau_b) \exp(-\tau_b/T_{2,\text{Rabi}})$ using Rabi frequency f_{Rabi} satisfying $\theta = 2\pi f_{\text{Rabi}}\tau_b$, Rabi-oscillation decay time $T_{2,\text{Rabi}}$, amplitude A , and offset B . Fitting $P(m, m_d)$ calculated from the acquired data to the above expression using a maximum likelihood method, we obtain $A = 0.311 \pm 0.006$, $B = 0.51 \pm 0.01$, $f_{R,0} = 85.1 \pm 0.9\%$, $f_{R,1} = 83 \pm 1\%$, $f_{d,R,0} = 95 \pm 1\%$, $f_{d,R,1} = 70.6 \pm 0.9\%$. The amplitude A relates solely to the initialization fidelity F_I as $F_I = A + 1/2$, yielding $F_I = 81.1 \pm 0.6\%$. The actual data of $P(m, m_d)$ and fit results are shown in Supplementary Note 2 for details of joint probability analyses.

Error analysis

All uncertainties represent 1σ confidence intervals obtained from fitting.

DATA AVAILABILITY

The data used to produce the figures in this work is available from the Zenodo repository at <https://doi.org/10.5281/zenodo.7870621>.

CODE AVAILABILITY

All the codes used in this work are available upon request to the authors.

REFERENCES

- Veldhorst, M. et al. An addressable quantum dot qubit with fault-tolerant control-fidelity. *Nat. Nanotechnol.* **9**, 981–985 (2014).
- Takeda, K. et al. A fault-tolerant addressable spin qubit in a natural silicon quantum dot. *Sci. Adv.* **2**, e1600694 (2016).
- Yoneda, J. et al. A quantum-dot spin qubit with coherence limited by charge noise and fidelity higher than 99.9%. *Nat. Nanotechnol.* **13**, 102–106 (2018).
- Noiri, A. et al. Fast universal quantum gate above the fault-tolerance threshold in silicon. *Nature* **601**, 338–342 (2022).
- Xue, X. et al. Quantum logic with spin qubits crossing the surface code threshold. *Nature* **601**, 343–347 (2022).
- Mills, A. R. et al. Two-qubit silicon quantum processor with operation fidelity exceeding 99%. *Sci. Adv.* **8**, eabn5130 (2022).
- Takeda, K. et al. Quantum tomography of an entangled three-qubit state in silicon. *Nat. Nanotechnol.* **16**, 965–969 (2021).
- Takeda, K., Noiri, A., Nakajima, T., Kobayashi, T. & Tarucha, S. Quantum error correction with silicon spin qubits. *Nature* **608**, 682–686 (2022).
- Philips, S. G. J. et al. Universal control of a six-qubit quantum processor in silicon. *Nature* **609**, 919–924 (2022).
- Yang, C. H. et al. Operation of a silicon quantum processor unit cell above one kelvin. *Nature* **580**, 350–354 (2020).
- Petit, L. et al. Universal quantum logic in hot silicon qubits. *Nature* **580**, 355–359 (2020).
- Maurand, R. et al. A CMOS silicon spin qubit. *Nat. Commun.* **7**, 13575 (2016).
- Zwerver, A. M. J. et al. Qubits made by advanced semiconductor manufacturing. *Nat. Electron.* **5**, 184–190 (2022).
- Camenzind, L. C. et al. A hole spin qubit in a fin field-effect transistor above 4 kelvin. *Nat. Electron.* **5**, 178–183 (2022).
- Fowler, A. G., Mariantoni, M., Martinis, J. M. & Cleland, A. N. Surface codes: Towards practical large-scale quantum computation. *Phys. Rev. A* **86**, 032324 (2012).
- Risté, D., Bultink, C. C., Lehnert, K. W. & Dicarlo, L. Feedback control of a solid-state qubit using high-fidelity projective measurement. *Phys. Rev. Lett.* **109**, 240502 (2012).
- Bushev, P. et al. Feedback cooling of a single trapped ion. *Phys. Rev. Lett.* **96**, 043003 (2006).
- Brakhane, S. et al. Bayesian feedback control of a two-atom spin-state in an atom-cavity system. *Phys. Rev. Lett.* **109**, 173601 (2012).
- Blumoff, J. Z. et al. Fast and high-fidelity state preparation and measurement in triple-quantum-dot spin qubits. *PRX Quantum* **3**, 010352 (2022).
- Mills, A. R. et al. High-fidelity state preparation, quantum control, and readout of an isotopically enriched silicon spin qubit. *Phys. Rev. Appl.* **18**, 064028 (2022).
- Kim, J. et al. Approaching ideal visibility in singlet-triplet qubit operations using energy-selective tunneling-based Hamiltonian estimation. *Phys. Rev. Lett.* **129**, 040501 (2022).
- Martinis, J. M. Qubit metrology for building a fault-tolerant quantum computer. *npj Quantum Inf.* **1**, 15005 (2015).
- Nakajima, T. et al. Quantum non-demolition measurement of an electron spin qubit. *Nat. Nanotechnol.* **14**, 555–560 (2019).
- Yoneda, J. et al. Quantum non-demolition readout of an electron spin in silicon. *Nat. Commun.* **11**, 1144 (2020).
- Xue, X. et al. Repetitive quantum nondemolition measurement and soft decoding of a silicon spin qubit. *Phys. Rev. X* **10**, 021006 (2020).
- Nakajima, T. et al. Coherence of a driven electron spin qubit actively decoupled from quasistatic noise. *Phys. Rev. X* **10**, 011060 (2020).
- Ralph, T. C., Bartlett, S. D., O'Brien, J. L., Pryde, G. J. & Wiseman, H. M. Quantum nondemolition measurements for quantum information. *Phys. Rev. A* **73**, 012113 (2006).
- Meunier, T. et al. Nondestructive measurement of electron spins in a quantum dot. *Phys. Rev. B* **74**, 195303 (2006).
- Elzerman, J. M. et al. Single-shot read-out of an individual electron spin in a quantum dot. *Nature* **430**, 431–435 (2004).
- Johnson, M. A. I. et al. Beating the thermal limit of qubit initialization with a Bayesian Maxwell's demon. *Phys. Rev. X* **12**, 041008 (2022).
- Connors, E. J., Nelson, J. J. & Nichol, J. M. Rapid high-fidelity spin-state readout in Si/Si-Ge quantum dots via rf reflectometry. *Phys. Rev. Appl.* **13**, 024019 (2020).
- Noiri, A. et al. Radio-frequency-detected fast charge sensing in undoped silicon quantum dots. *Nano Lett.* **20**, 947–952 (2020).
- Eng, K. et al. Isotopically enhanced triple-quantum-dot qubit. *Sci. Adv.* **1**, e1500214 (2015).

ACKNOWLEDGEMENTS

This work was supported financially by Core Research for Evolutional Science and Technology (CREST), Japan Science and Technology Agency (JST) (JPMJCR15N2 and JPMJCR1675), PRESTO grant Nos. JPMJPR2017 and JPMJPR21BA, MEXT Quantum Leap Flagship Program (MEXT Q-LEAP) grant No. JPMXS0118069228, JST Moonshot R&D grant no. JPMJMS226B, and JSPS KAKENHI grant Nos. 17K14078, 18H01819, 19K14640, 20H00237, 22H01160, 23H01790, and 23H05455.

AUTHOR CONTRIBUTIONS

T.K. carried out the experiments and analyzed the data with input from T.N., K.T., A.N., and J.Y., T.N. programmed the DSP. T.K. programmed the sequencer with input from T.N. K.T., A.N., and J.Y. set up the measurement hardware. K.T. fabricated the device. S.T. supervised the project. All authors discussed the results. T.K. wrote the manuscript with contributions from all authors.

COMPETING INTERESTS

The authors declare no competing interests.

ADDITIONAL INFORMATION

Supplementary information The online version contains supplementary material available at <https://doi.org/10.1038/s41534-023-00719-3>.

Correspondence and requests for materials should be addressed to T. Kobayashi.

Reprints and permission information is available at <http://www.nature.com/reprints>

Publisher's note Springer Nature remains neutral with regard to jurisdictional claims in published maps and institutional affiliations.



Open Access This article is licensed under a Creative Commons Attribution 4.0 International License, which permits use, sharing, adaptation, distribution and reproduction in any medium or format, as long as you give appropriate credit to the original author(s) and the source, provide a link to the Creative Commons license, and indicate if changes were made. The images or other third party material in this article are included in the article's Creative Commons license, unless indicated otherwise in a credit line to the material. If material is not included in the article's Creative Commons license and your intended use is not permitted by statutory regulation or exceeds the permitted use, you will need to obtain permission directly from the copyright holder. To view a copy of this license, visit <http://creativecommons.org/licenses/by/4.0/>.

© The Author(s) 2023